Can one reconcile the classical theories and the WISHE-theories of tropical cyclone intensification?

Roger K. Smith[a]*, Michael T. Montgomery[b] and Shanghong Wang[c]
[a] *Meteorological Institute, Ludwig-Maximilians-Universität in Munich, Germany*
[b] *Dept. of Meteorology, Naval Postgraduate School, Monterey, CA, USA*
[c] *Shanghai Typhoon Institute, China Meteorological Administration, Shanghai, China and Asia-Pacific Typhoon Collaborative Research Center, Shanghai, China*
*Correspondence to: Prof. Roger K. Smith, Meteorological Institute, Ludwig-Maximilians University of Munich, Theresienstr. 37, 80333 Munich. E-mail: roger.smith@lmu.de

An effort is made to reconcile the classical theories of tropical cyclone intensification by Shapiro and Willoughby and Schubert and Hack and the various prognostic (or WISHE-) theories of Emanuel. As a start, it proves necessary to extend the classical theories to account for explicit latent heat release in slantwise ascending air. While such an effort uncovers enroute a range of old modelling issues concerning the representation of deep convection in a balance framework, the analysis provides a new perspective of these issues. The bottom line is that the two theories cannot be reconciled.

The behaviour of the model with explicit latent heat release is illustrated by a particular calculation starting with an axisymmetric vortex in a conditionally-unstable atmosphere. As soon as condensation occurs aloft, the moist Eliassen equation for the overturning circulation becomes hyperbolic in the convectively-unstable region and the model cannot be advanced forwards beyond this time unless the Eliassen equation is suitably regularized to remove these hyperbolic regions. However, regularization suppresses buoyant convection, leaving no mechanism to reverse the frictionally-induced outflow in the lower troposphere required to concentrate absolute angular momentum there. For this reason, the initial vortex spins down, even following the formation of elevated cloud with the accompanying latent heat release.

The fact that the flow configuration in the moist version of the classical theories is similar to that in the WISHE-theories raises several fundamental questions concerning the physics of vortex spin up in the WISHE-theories, calling into question the integrity of these theories, themselves.

Key Words: Hurricane; tropical cyclone; typhoon; classical intensification theories; WISHE intensification theories, Eliassen equation

Received January 24, 2024; Revised ; Accepted

Citation: . . .

1. Introduction

Building on the seminal studies of the thermally or frictionally controlled meridional circulation in a circular vortex and of frontal circulations by Eliassen (1951, 1962), Willoughby (1979), Shapiro and Willoughby (1982), Schubert and Hack (1982), Schubert and Hack (1983) and Schubert and Alworth (1982) developed similar theories for the diagnosis and evolution of the balanced tangential and overturning circulation of a tropical cyclone. The underlying premise of the theories, supported by a scale analysis of the governing equations, is that the cyclone

remains in hydrostatic and gradient wind balance as it evolves. With this assumption, one obtains a linear second-order partial differential equation for the streamfunction of the overturning circulation, forced by prescribed heat and momentum sources that, without such a circulation, would act immediately to destroy balance. When this equation is globally elliptic, one obtains a well posed formulation for the balanced evolution of an intensifying vortex. These classical theories highlighted the role of the overturning circulation in promoting tropical cyclone spin up by converging absolute angular momentum surfaces in the lower troposphere. In the diagnostic formulations of Shapiro and Willoughby (1982) and Schubert and Hack (1982), vortex spin up was inferred from the tangential wind or potential temperature tendencies brought about by the overturning circulation.

More recently, inspired by the foregoing studies, Smith et al. (2018) constructed a prognostic balance model to further explore how a tropical cyclone in such a model evolves in time. Using diabatic heating rates suggested by numerical model simulations of intensifying tropical cyclones, it was shown that, on a time scale of half a day, the partial differential equation for the streamfunction of the overturning circulation, now referred to as the Eliassen equation*, develops regions in which it becomes hyperbolic. Thereafter, the model solution can be continued only if the coefficients of the Eliassen equations are "suitably" modified to keep the equation globally elliptic. We refer to such modification as a regularization procedure following Möller and Shapiro (2002) and note that any such procedure is intrinsically *ad hoc*.

Typically, regularization allows the solution to be continued for a further 12-24 hours before a catastrophic breakdown ensues. This breakdown appears to be coupled with the rapid onset of centrifugal (inertial) instability as the region requiring regularization becomes comparatively large. Smith et al. showed that such instability is not eliminated by regularization. Various issues associated with the regularization procedure, itself, were investigated by Wang and Smith (2019), Montgomery and Persing (2020) and Wang and Smith (2021).

The solutions of the prognostic balance balance model remain smooth and usable, even beyond the time at which the Eliassen equation has to be regularized, up to perhaps an hour before the ultimate breakdown of the solution occurs. For this reason, the prognostic balance model was chosen by Smith and Wang (2018) to highlight the separate roles of diabatic heating and boundary layer friction within a balance framework.

From a scientific viewpoint, one important limitation of the foregoing prognostic balance model is *the specification of* the distribution of diabatic heating rate, which circumvents the need for considering explicit moisture and sources of moisture. For greater realism, the distribution and magnitude of the heating should be determined as part of the solution and the supply of moisture from the ocean should be included also. A possible way to accomplish this was outlined by Montgomery and Smith (2022), a study that sought to relate the widely accepted wind-induced surface heat exchange (WISHE) paradigm for tropical cyclone intensification (Emanuel 1995, 1997, 2012) to the classical balance formulation envisaged by Shapiro and Willoughby and by Schubert and collaborators. Like the classical theories, the WISHE-theories invoke hydrostatic and gradient wind balance also, but incorporate a fundamentally different representation of moist processes and they take explicit account of the surface moisture source.

The Montgomery and Smith (2022) formulation of the moist problem was generalized by Smith and Montgomery (2023) (see Section 16.1) to account for the possibility of moist slantwise ascent, allowing for a closer comparison with the Emanuel formulations that purport to underpin the WISHE feedback mechanism. The generalization suggested two possibilities for balanced vortex evolution in the moist problem, but Smith and Montgomery stopped short of solving the moist problem, itself.

The first possibility above is that the Eliassen equation in regions of latent heat release remains elliptic with a small, but positive effective static stability. The second possibility is that the equation becomes parabolic or hyperbolic in such regions. In the former case, it was demonstrated that the inflow in the frictional boundary layer would force outflow throughout the troposphere above this layer so that the tangential wind in the moist region would inevitably spin down. In the latter case, it was argued that the inclusion of explicit latent heat release was incompatible with the assumption of local hydrostatic balance. Therefore, to retain the integrity of a balance formulation, convective instability would have to be removed by implementing some cumulus parameterization scheme. Indeed, it was proposed that only by incorporating such a parameterization scheme would it be possible in a balance framework to reverse the outflow induced by boundary layer friction to inflow in the lower troposphere to produce vortex spin up there.

In Section 16.7.1 of the book, Smith and Montgomery arrived at conflicting conclusions regarding into which of the former cases the WISHE-theories fit, noting that "At the time of writing, the consequences of these conflicting conclusions concerning Emanuel's later intensification theories remain to be understood". They went on to say that that: " ... we are led to tentatively conclude that they (i.e., the WISHE-theories) are incompatible with the classical balance theory of Eliassen".

One purpose of the present paper is to demonstrate that the balance model with explicit latent heat release falls *strictly* in the second case discussed above. Another purpose is to apply the understanding gained from the analyses of this model to sharpen our understanding of the relationship between the classical balance theories of tropical cyclone intensification and the WISHE-theories. One notable difference between the two theories is the different vertical structure of the secondary overturning circulation, the reasons for which remain obscure.

2. The prognostic balance equations

Classical axisymmetric balance theory is based on the tendency equations for tangential velocity component, v, and some thermodynamical quantity such as the potential temperature, θ, or its inverse together with a constraint equation for thermal wind balance and one for mass continuity in the quasi-static approximation that neglects acoustic waves. In a cylindrical coordinate system (r, z) on an f-plane, Smith et al. (2018) wrote the foregoing

*Sometimes referred to also as the Sawyer-Eliassen equation.

equations in the form

$$\frac{\partial v}{\partial t} = -u\frac{\partial v}{\partial r} - w\frac{\partial v}{\partial z} - \frac{uv}{r} - fu - \dot{V}, \tag{1}$$

$$\frac{\partial \chi}{\partial t} + u\frac{\partial \chi}{\partial r} + w\frac{\partial \chi}{\partial z} = -\chi^2\dot{\theta}, \tag{2}$$

$$\frac{\partial}{\partial r}\ln\chi + \frac{C}{g}\frac{\partial}{\partial z}\ln\chi = -\frac{\xi}{g}\frac{\partial v}{\partial z}, \tag{3}$$

$$\frac{\partial \rho r u}{\partial r} + \frac{\partial \rho r w}{\partial z} = 0, \tag{4}$$

where u and w are the radial and vertical velocity components, t is the time, f is the Coriolis parameter (assumed constant), ρ is the density, $\dot{V}$ is the tangential momentum sink associated with the near-surface frictional stress, $\chi = 1/\theta$ is the inverse of potential temperature, $\dot{\theta} = d\theta/dt$ is the material derivative of the dry potential temperature (i.e., the diabatic heating rate), $C = v^2/r + fv$ is the sum of centrifugal and Coriolis forces per unit mass, $\xi = f + 2v/r$ is twice the local absolute angular velocity and g is the effective gravitational acceleration. Here, the steady form of the continuity equation (Eq. (4)) is chosen as appropriate for a slowly-evolving balance flow which does not excite acoustic waves.

The transverse velocity components u and w are obtained in terms of a streamfunction for the transverse overturning circulation, ψ, to ensure that the quasi-static form of the continuity equation is identically satisfied, i.e.,

$$u = -\frac{1}{\rho r}\frac{\partial \psi}{\partial z}, w = \frac{1}{\rho r}\frac{\partial \psi}{\partial r}. \tag{5}$$

2.1. The Eliassen equation

The Eliassen equation for ψ is obtained by differentiating the thermal wind equation (Eq. (3)) with respect to time and eliminating the time derivatives of v and χ using Eqs. (1) and (2). After some algebra, one obtains

$$\frac{\partial}{\partial r}\left[\gamma\left(N^2\frac{\partial \psi}{\partial r} - B\frac{\partial \psi}{\partial z}\right)\right] + \frac{\partial}{\partial z}\left[\gamma\left(I_g^2\frac{\partial \psi}{\partial z} - B\frac{\partial \psi}{\partial r}\right)\right] = g\frac{\partial}{\partial r}\left(\chi^2\dot{\theta}\right) + \frac{\partial}{\partial z}\left(C\chi^2\dot{\theta}\right) + \frac{\partial}{\partial z}\left(\chi\xi\dot{V}\right), \tag{6}$$

where $\gamma = \chi/\rho r$, $N^2 = -(g/\chi)\partial\chi/\partial z$ represents the *static stability*, $B = (1/\chi)(\partial(\chi C)/\partial z)$ represents the *baroclinicity*, $I_g^2 = \xi\zeta_a + (C/\chi)\partial\chi/\partial r$ represents the *generalized inertial (centrifugal) stability*, $\zeta_a = \zeta + f$ is the absolute vorticity and $\zeta = (1/r)\partial(rv)/\partial r$ is the vertical component of relative vorticity.

The Eliassen equation, Eq. (6), is a linear second-order partial differential equation with the discriminant, D, given by

$$D = 4\gamma^2\left(I_g^2N^2 - B^2\right), \tag{7}$$

and it is elliptic if $D > 0$.

In essence, the Eliassen equation determines the streamfunction required to keep the tangential circulation in thermal wind balance at every location in the presence of heating and friction that would otherwise act to move it away from balance.

2.2. The moist Eliassen equation

In cloudy regions, condensation of water vapour or evaporation of liquid water occurs at a rate proportional to the material rate-of-change, d/dt, of saturation mixing ratio, r_v^*. The largest contribution to this quantity arises from vertical motions in the cloud, although if the cloud is tilted, radial motions may make a non-negligible contribution. In turn, the material rate-of-change of latent heating or cooling is $\dot{Q} = -L_v dr_v^*/dt$, where L_v is the latent heat of vaporization. Finally, the diabatic heating rate, $\dot{\theta}$, may be approximated by[†]

$$\dot{\theta} = \frac{\dot{Q}}{c_p\pi} \approx -\frac{L_v}{c_p\pi}\left(u\frac{\partial r_v^*}{\partial r} + w\frac{\partial r_v^*}{\partial z}\right), \tag{8}$$

where, c_p is the specific heat of dry air at constant pressure and π is the Exner function defined by $\pi = (p/p_{**})^\kappa$, p is the pressure, p_{**} is a reference pressure of 1000 mb, $\kappa = R/c_p$, and R is the specific gas constant for dry air. Here, for simplicity, the additional heating or cooling associated with ice freezing or sublimation are not considered.

Then using the streamfunction ψ with u and w obtained from Eq. (5), Eq. (8) gives,

$$\chi^2\dot{\theta} = -\frac{L_v\chi^2}{c_p\pi}\left(-\frac{\partial r_v^*}{\partial r}\frac{1}{\rho r}\frac{\partial \psi}{\partial z} + \frac{\partial r_v^*}{\partial z}\frac{1}{\rho r}\frac{\partial \psi}{\partial r}\right), \tag{9}$$

The modified Eliassen equation for moist slantwise ascent or descent in cloudy air is obtained by substituting for $\dot{\theta}$ from Eq. (9) into Eq. (6). After a little algebra one obtains,

$$\frac{\partial}{\partial r}\left[\gamma\left\{\left(N^2+\frac{gL_v}{c_{pd}T}\frac{\partial r_v^*}{\partial z}\right)\frac{\partial \psi}{\partial r} - \left(B+\frac{gL_v}{c_{pd}T}\frac{\partial r_v^*}{\partial r}\right)\frac{\partial \psi}{\partial z}\right\}\right] + \frac{\partial}{\partial z}\left[\gamma\left\{\left(I_g^2 - \frac{CL_v}{c_{pd}T}\frac{\partial r_v^*}{\partial r}\right)\frac{\partial \psi}{\partial z} - \left(B - \frac{CL_v}{c_{pd}T}\frac{\partial r_v^*}{\partial z}\right)\frac{\partial \psi}{\partial r}\right\}\right] = \frac{\partial}{\partial z}\left(\chi\xi\dot{V}\right), \tag{10}$$

where T is the air temperature.

The generalized discriminant of the moist Eliassen equation, D_m, is given by

$$D_m = 4\gamma^2\left(I_g^2 - \frac{CL_v}{c_pT}\frac{\partial r_v^*}{\partial r}\right)\left(N^2 + \frac{gL_v}{c_pT}\frac{\partial r_v^*}{\partial z}\right) - 4\gamma^2\left\{B + \frac{L_v}{2c_pT}\left(g\frac{\partial r_v^*}{\partial r} - C\frac{\partial r_v^*}{\partial z}\right)\right\}^2. \tag{11}$$

Of course, both Eq. (10) and Eq. (11) reduce to Eq. (6) and Eq. (7), respectively, if there is no condensation, equivalent to setting $L_v = 0$ in Eq. (9).

Compared to the Eliassen equation (6), the modified Eliassen equation only has one forcing term on the right

[†]The retention of the local time derivative term adds a time derivative "forcing" term to the right hand side of the corresponding Eliassen equation. This forcing term corresponds to a higher order term in the balance formulation, which would be typically neglected for slowly evolving vortices (see e.g., Smith and Montgomery (2023), Section 5.13.5). A scale analysis and our own *a posteriori* calculations confirm that this term is subdominant in comparison to the radial and vertical advection of r_v^*.

hand side, the one associated with tangential friction in the vortex boundary layer. As noted in Montgomery and Smith (2022), when the friction vanishes the only solution is a zero streamfunction provided the generalized discriminant is positive.

2.3. Determination of cloudy regions, the moisture equation

The fact that the moist Eliassen equation (10) for cloudy air reduces to the more conventional form, Eq. (6), with $\dot{\theta} = 0$ outside of cloud means that it can be solved globally, simply by setting $L_v = 0$ in regions outside of cloud. To determine whether air in a particular location is cloudy or not requires simply a knowledge of the local water vapour mixing ratio, r_v in relation to the saturation mixing ratio at that point, which is a function only of the local pressure and temperature, or equivalently pressure and χ. Simply, non-cloudy regions are where $r_v < r_v^*$ and regions of cloud are where $r_v = r_v^*$. Clearly we need to know the spatial distribution of r_v at any time, so that in a prognostic system, we require to know the initial distribution of r_v and to have a prognostic equation for r_v. The prognostic equation may be written as

$$\frac{\partial r_v}{\partial t} = -u\frac{\partial r_v}{\partial r} - w\frac{\partial r_v}{\partial z} + \dot{R}_v, \qquad (12)$$

where $\dot{R}_v$ is the source of water vapour expressed in terms of mixing ratio (see below).

2.4. The solution method

The solution method is similar to that described by Smith et al. (2018) and involves the following steps.

1 Given the initial spatial distribution of v, say $v_o(r, z)$ in some domain $(0 \le r \le R, 0 \le z \le Z)$, and a far-field thermodynamic sounding for pressure as a function of height, $p(R, z)$, calculate the initial distribution of χ, say $\chi_o(r, z)$, from Eq. (3) using the method described by Smith (2006). As a by product of this solution, one obtains the initial pressure distribution $p_o(r, z)$ because the characteristics of the first-order partial differential equation (3) are just the isobars.

2 Knowledge of $p_o(r, z)$ and $\chi_o(r, z)$ enables the initial distribution of r_v^*, say $r_{vo}^*(r, z)$, to be determined and given the initial spatial distribution of r_v, say $r_{vo}(r, z)$, one can determine which, if any, regions of the domain are cloudy. If at any points, $r_v > r_{vo}^*$, we set $r_v = r_{vo}^*$.

3 Knowledge of the cloudy and cloud-free regions enables the modified Eliassen equation (10) to be solved for the initial streamfunction, say $\psi_o(r, z)$, as long as the equation is globally elliptic, i.e., $D_m > 0$ everywhere. See below if this is not the case.

4 Now, the velocity components of the overturning circulation at the initial time, say $u_o(r, z)$ and $w_o(r, z)$, can be obtained from Eqs. (5).

5 At this stage, all quantities are available at the initial time so that the prognostic equations (1) and (12) may be used to determine the quantities at some small future time, $t = \Delta t$, by approximating, for example by $v(r, z, \Delta t)$ by $v(r, z, 0) + (\partial v/\partial t)_{t=0}\Delta t$.

6 With the knowledge of v and r_v at time Δt, steps [1] to [5] may be repeated successively to advance the solution to any desired time, $t = n\Delta t$ where n is an integer, the proviso being that at each time step, D_m remains everywhere positive.

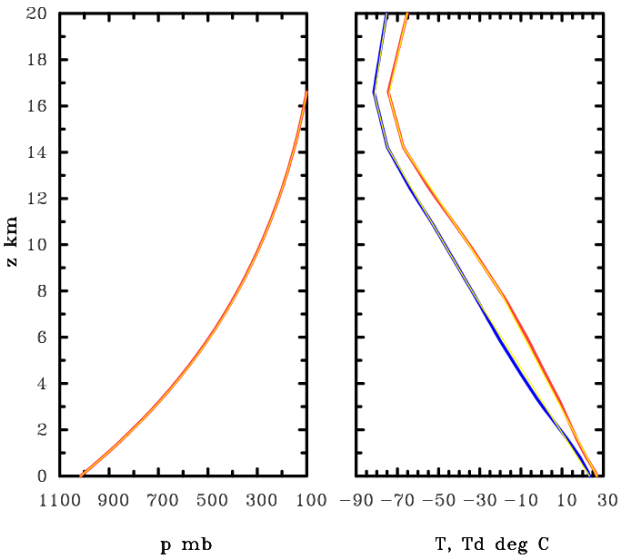

Figure 1. Presssure, temperature and dewpoint temperature as a function of height in the Dunion moist tropical sounding for the Atlantic Hurricane season. Solid red and blue curves depict the actual Dunion sounding, while the thinner yellow curves show the piecewise linear approximation to this sounding.

In the foregoing model it should be noted that Eq. (2) is used only to derive Eq. (10) and not used to predict χ. In principle, an alternative would be to predict χ using Eq. (2) and to diagnose v from the balance condition (3), but because Eq. (3) is quadratic in v, a real solution may not exist everywhere.

If regions develop in which $D_m \le 0$, Eq. (10) is solvable diagnostically as an elliptic equation only if the coefficients are regularized in these regions. As noted in the Introduction, strategies for regularization, which are necessarily *ad hoc*, and the consequences of regularization concerning the integrity of the solutions, are explored by Wang and Smith (2019), Montgomery and Persing (2020) and Wang and Smith (2021).

2.5. The formulation for $\dot{R}_v$

The remaining task for implementing the solution is the formulation for $\dot{R}_v$ in Eq. (12). One possibility would be to express $\dot{R}_v$ as a vertical diffusion term and implement a surface boundary condition on r_v to allow surface moisture fluxes to elevate r_v in the region where surface wind speeds are high. A less sophisticated method, adequate for the present purposes, is to simply take $\dot{R}_v = 0$. This choice is justified (i) because the ambient sounding used (see below) has adequate convective available potential energy and minimal convective inhibition for convection to be initiated, at least in principle, (ii) because the integrity of the solution becomes increasingly questionable after condensation occurs aloft, breaking down on a time-scale of an hour after this occurrence, and (iii) because, as shown in Section 4.2 below, even if included, surface moisture fluxes would be rapidly shut down by a near surface layer

of saturated air that forms in the solution. In any case, our main focus is on the behaviour of the balance model after condensation occurs and latent heat is released.

3. A specific calculation

The calculation described here uses a domain size $R = 1000$ km in radius and $Z = 20$ km in height with a radial grid spacing of 5 km and a vertical grid spacing of 200 m. The Coriolis parameter, f, corresponds with a latitude of 20^{o}N. The calculation begins with an initial warm-cored vortex with tangential wind profile given by the formula

$$v(r) = V_{max} s \exp[-(1 - s^b)/b] \cos(bz), \qquad (13)$$

where $s = r/R_{Vmax}$, r is the radius, $b = \frac{1}{2}\pi/Z$, z is the height, V_{max} is the maximum tangential velocity and R_{Vmax} is the radius of this maximum. At the initial time, V_{max} = 40 m s^{-1} and R_{Vmax} = 60 km. The large initial velocity was chosen to initiate cloud formation within a short period of time and with the expectation that the vortex would decay with time. Calculations for weaker initial vortices are discussed also.

The initial thermodynamic sounding at the outer side boundary, $r = R$ is based on a piecewise linear approximation of the temperature and dewpoint temperature of the Dunion mean tropical sounding for the Atlantic hurricane season (Dunion 2011). The corresponding pressure distribution is calculated using the hydrostatic equation using the surface pressure of the actual sounding, 1015.3 mb. Figure 1 shows the linear approximation to the sounding compared with the actual sounding.

The formulation of frictional stress is similar to that employed in Montgomery and Smith (2022). In the formulation, the effects of surface friction are represented by a body force per unit mass in the tangential direction corresponding with the surface frictional stress distributed through a layer with depth H. The body force has the spatial form

$$\dot{V}(r, z) = \frac{C_d}{H} v_s^2 \left(1 - \frac{z}{H_1}\right)^2 (0 \le z \le H_1), \qquad (14)$$

where C_d is the surface drag coefficient (assumed here to be a constant equal to 2×10^{-3}) and $v_s = v_s(r, 0, t)$ is the tangential wind component at the surface at time t. The constants H and H_1 are 500 m and 2000 m, respectively, and are chosen so that the inflow occurs within a surface-based layer about 1 km in depth as is observed.

The prognostic element of the calculation represented by Eqs. (1) and (12) uses a time step of 1 minute. For simplicity, the initial water vapour mixing ratio distribution is taken to be the same at all radii, equal to that at the side boundary.

4. Results

Figure 2a shows a time series of the maximum tangential wind component, V_{max}, the location of which becomes slightly elevated as time proceeds. Despite the need to regularize the Eliassen equation from 62 minutes onwards, the decay rate of V_{max} is approximately linear for the duration of the calculation, which extends to 146 minutes. This decay occurs even in the presence of cloud formation and latent heat release as the flow evolves and it was anticipated in the analysis outlined by (Montgomery and Smith 2022, their Figure 4 and subsection 2.4.2). The significance of this result is addressed below, as is the nature of the solution breakdown.

The steady decrease in V_{max} is accompanied, of course, by a progressive decline in the strength of the frictionally-driven overturning circulation as evidenced by the decline in U_{max} and U_{min} shown in Fig. 2b. Before regularization is required, the rate-of-decline of these two quantities is approximately linear, but it levels off after this time and there is a period of increase after about 80 minutes in which U_{max} develops fluctuations while increasing slightly in a time mean. The fluctuations in U_{max} are associated with small scale features in the fields, probably consequences of regularization, that lead ultimately to solution breakdown (see Subsection 4.4).

Figures 3 and 4 show radius-height cross sections of various fields below an altitude of 5 km at selected times. The left panels of Fig. 3 show the tangential and radial velocity components as well as contours of absolute angular momentum, $M = rv + \frac{1}{2}fr^2$ at the initial time, at 60 minutes, just two minutes before regularization of the moist Eliassen equation is required, and at 90 minutes, 56 minutes before the solution breaks down and prior to most fields losing their relatively smooth character. The right panels of Fig. 3 show the vertical velocity component at the same times.

4.1. Kinematic fields

The principal features of the velocity fields in Fig. 3 are similar to those described in the friction-only simulation in Section 4d of Smith et al. (2018) and Section 2.3.1 of Montgomery and Smith (2022). At the initial instant, there is a shallow layer of inflow below about 1 km in altitude and a deeper layer of outflow above. The maximum inflow occurs at the surface at a radius of about 200 km and the maximum outflow occurs at about the same radius and an altitude just below 2 km, although outflow extends throughout the entire troposphere (not shown). By construction, the maximum tangential velocity component occurs at the surface at this time. In the part of the calculation domain shown, there is mostly ascent, with subsidence into the boundary layer evident at low levels beyond a radius of 275 km. The depth of this subsidence layer increases with radius. Significantly, the maximum ascent occurs between about 1 and 2 km in altitude, below the level of maximum outflow and near to the radius of maximum tangential velocity. This is, of course, where one would expect cloud to form first.

The foregoing features persist as the flow evolves, the main difference being the progressive elevation in the location of V_{max} as the tangential wind is reduced near the surface by the tangential frictional force and the progressive weakening of the overturning circulation. As illustrated by the left panels in Fig. 3, the decay of the vortex circulation is associated with the outward movement of the M-surfaces above the frictional inflow layer, altitudes at which the quantity M is materially conserved (see e.g., Smith and Montgomery 2023, Section 6.1).

The localized regions surrounding the location of maximum outflow in Fig. 3e and maximum vertical velocity

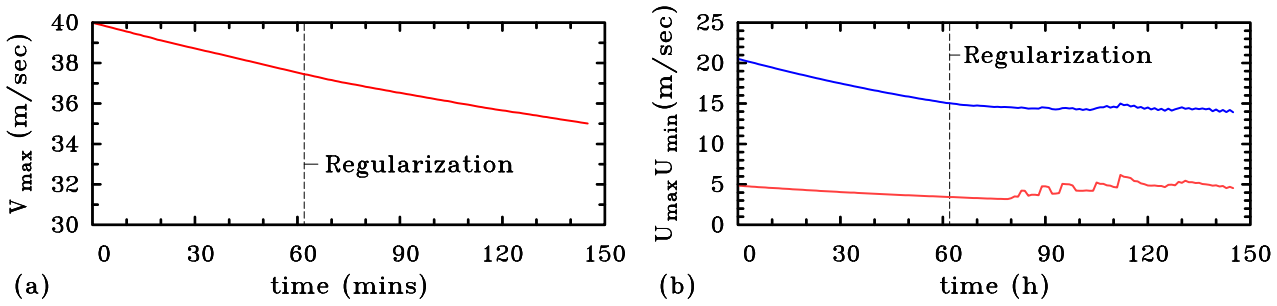

Figure 2. Time evolution of (a) V_{max} (t), (b) Umax (t) (red), $U_{min}(t)$ (blue), for the moist balanced vortex. The vertical dashed line indicates the first time at which the discriminant in the Eliassen equation first becomes negative.

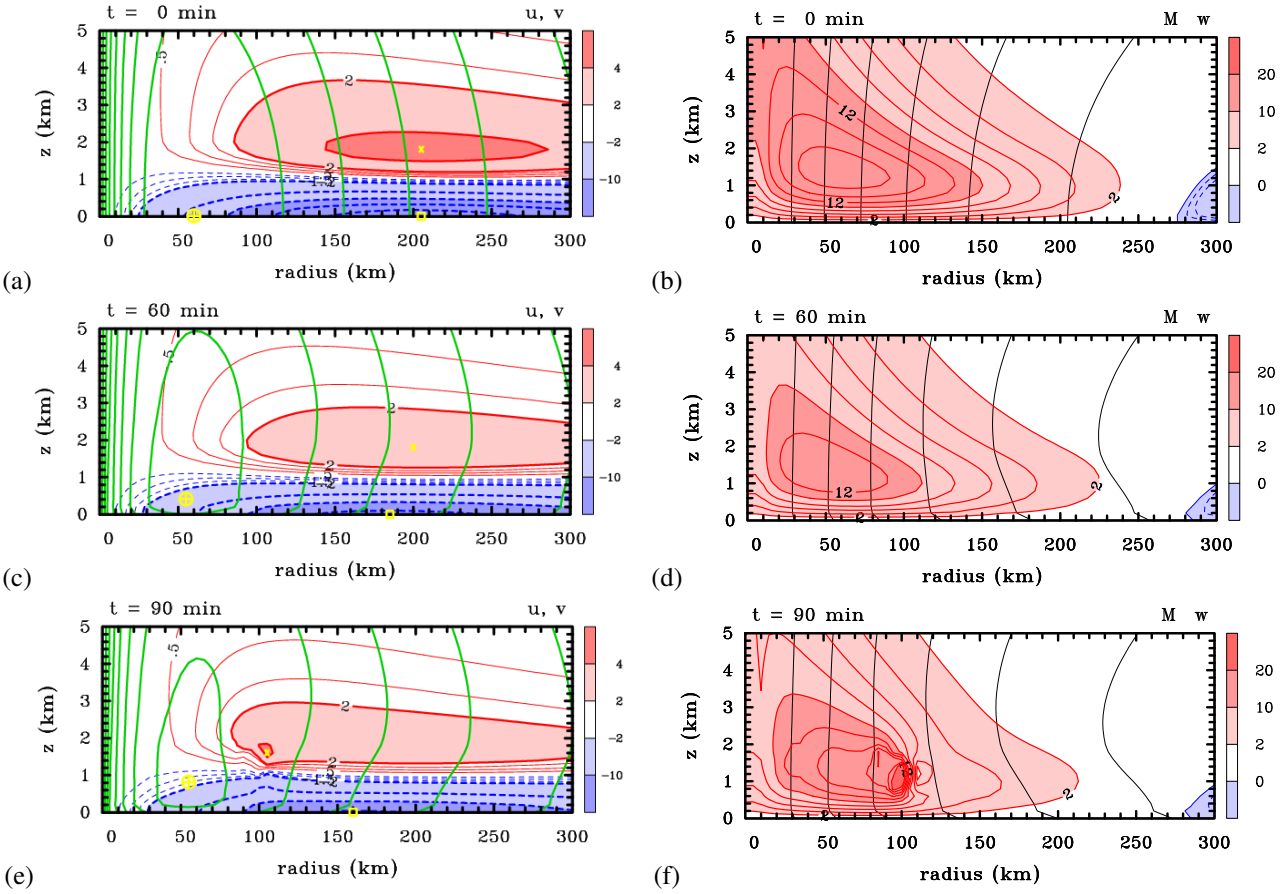

Figure 3. Radial-height cross sections of (a,c,e) contours of tangential velocity, v, and radial velocity u (shaded), and (b,d,f) contours of vertical velocity, w (shaded) and M-surfaces at (a,b) the initial time, (c,d) 60 minutes and (e,f) at 90 minutes. Only the inner and lower part of the calculation domain are shown. Contour intervals: for v, 10 m s^{-1}; for u, thick contours 2 m s^{-1} for positive values and 4 m s^{-1} for negative values, thin contours 0.5 m s^{-1} for $|u| \leq 1.5$ m s^{-1}; for w 2 cm s^{-1}; for M 1×10^6 m^2 s^{-1}. Solid contours for positive values, dashed contours for negative values. The yellow symbols in (a), (c) and (e) indicate the locations of maximum v, ($\oplus$), maximum u, ($\times$) and minimum u, ($\square$).

in Fig. 3f at 90 minutes are signs of some kind of local breakdown of the solution. We surmise that these are a consequence of regularizing the Eliassen equation and are most likely unphysical.

4.2. Formation of cloud and convective instability

The left panels of Fig. 4 show radius-height cross sections of the relative humidity field (RH) and the right panels show cross sections of potential temperature, θ, and the discriminant of the moist Eliassen equation, D_m, at the same times as in Fig. 3. For reference, all panels show the M-surfaces, again as in Fig. 3.

At the initial time, the flow is everywhere unsaturated. In a shallow layer near the surface, the relative humidity increases slightly with decreasing radius. This increase is related to cooler temperatures associated with the lower pressure in the vortex inner core[‡]. Above this layer, the relative humidity decreases with decreasing radius on

[‡]Note that the initial vortex profile used here is approximately barotropic near the surface and the barotropic vortex is cold cored (see e.g., Smith and Montgomery 2023, Section 5.3).

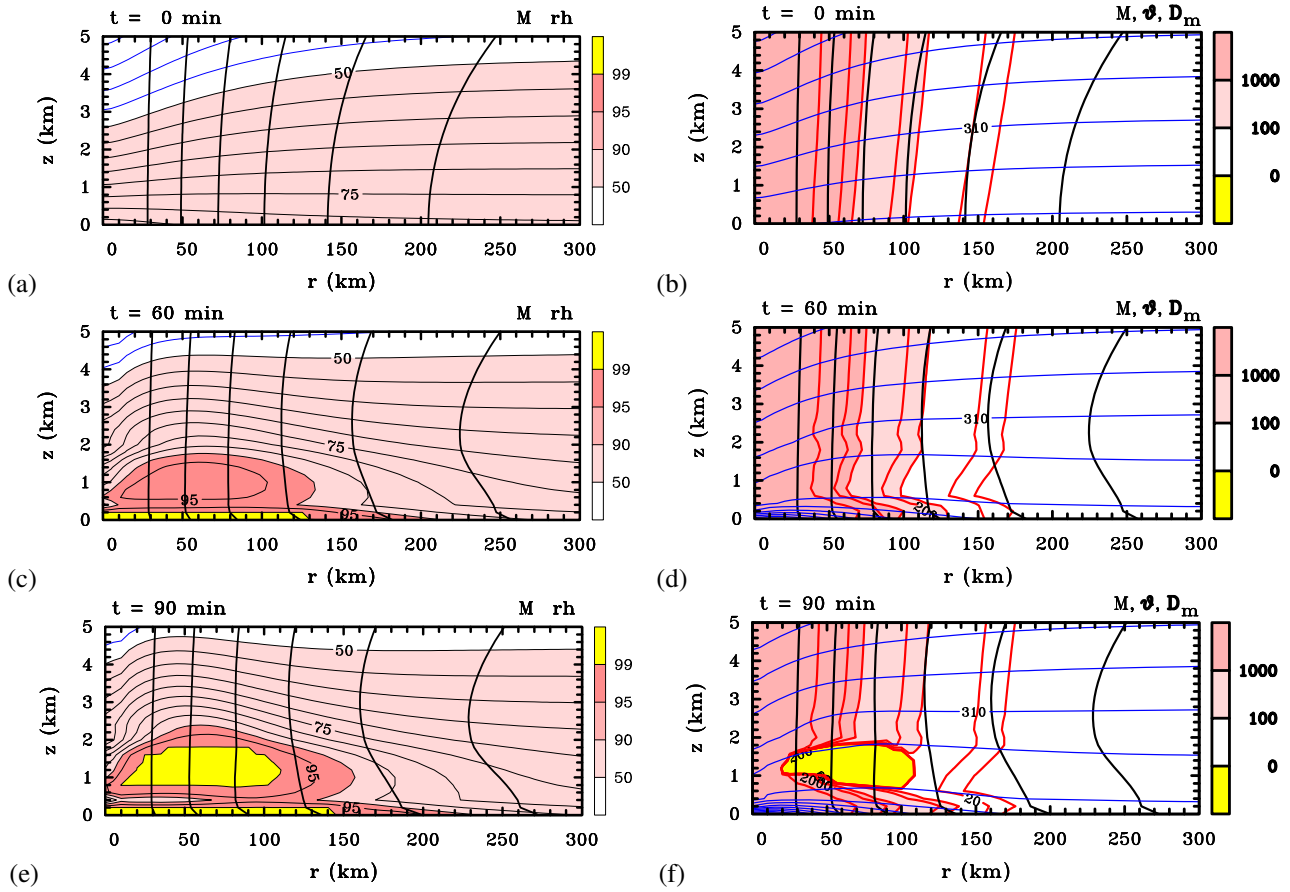

Figure 4. Radial-height cross sections of M-surfaces superimposed on (a,c,e) contours of relative humidity, RH (shaded), and (b,d,f) contours of potential temperature, θ, and Eliassen equation discriminant, D_m (shaded) at (a,b) the initial time, (c,d) 60 minutes and (e,f) at 90 minutes. Contour intervals: for RH, 5%; for M, 1×10^6 m^2 s^{-1} starting from the left at 1 of these units; for θ, 10 K. Since values of D_m vary radially by several orders of magnitude, a logarithmic scale has been used, beginning with a value 1×10^{-27} kg^{-2} m^4 s^{-4} K^{-2}. In multiples of this base value, the contours shown are from right to left: 1, 10, 20, 100, 200, 1000, 2000, 10^4.

account of the warm core aloft, which is evident in the lowering of the isentropes near the axis as seen in Fig. 4b.

As time proceeds, the tangential velocity is reduced near the surface due to surface friction, whereupon the positive increase in the tangential velocity with height in conjunction with the thermal wind balance constraint leads to strong cooling near the surface. The cooling is reflected in the formation of a strong surface-based stable layer in the pattern of isentropes in Fig. 4b. This feature is not realistic, of course, but rather an unrealistic thermodynamic feature of the balance boundary approximation. A consequence of the cooling is the formation of a surface-based layer of saturated air, essentially a layer of fog, in the inner core of the vortex (Fig. 4b). Saturation occurs first at 18 minutes at the surface and at an altitude of 200 m at radii between 10 and 55 km. As time proceeds, the saturated layer expands in radius, but does not become thicker (not shown). This "foggy layer" precedes the formation of cloud in the region of strongest ascent aloft, but its occurrence is not connected with instability in the sense that it is not accompanied by a negative discriminant of the moist Eliassen equation.

Saturation leading to an elevated cloud above the foggy layer begins at 62 minutes and leads immediately to convective instability such that the coefficient multiplying the derivative $\partial^2\psi/\partial r^2$ in the moist Eliassen equation becomes negative. As a result, the discriminant of the equation becomes negative in this region. In order to continue the solution beyond this time as an elliptic problem, it is necessary to regularize the Eliassen equation by modifying one or more of the coefficients of the highest-order derivatives in regions where $D_m < 0$ to render D_m small, but positive. Any such procedure is necessarily *ad hoc* and its success has to be judged with caution. Regularization may be reasonable if the region(s) of negative D_m are comparatively small in area, but may be problematic when the area becomes appreciable. By "reasonable" we mean that the solution outside the regularized region looks reasonable subjectively. As noted above, the various issues accompanying regularization are explored by Wang and Smith (2019), Montgomery and Persing (2020) and Wang and Smith (2021).

In the present problem, it is the moist stability term, $N^2 + gL_v\partial r_v^*/\partial z/(c_pT)$, which in a linear approximation is proportional to $\partial\theta_e^*/\partial z$, that first leads to a region of negative D_m when cloud forms aloft. At 90 minutes, for example, the region of negative D_m is indicated in yellow in Fig. 4f and this region coincides approximately with the elevated region of saturated air shown in Fig. 4e. The regularization procedure adopted here is to replace the negative values of $N^2 + gL_v\partial r_v^*/\partial z/(c_pT)$ by small positive values sufficient to make D_m small and positive in the convectively unstable region.

While the foregoing procedure allows the solution to be continued for more than an hour after the shallow cloud has formed, it is clearly masking the physics of the problem. In reality, the cloudy air becomes convectively

unstable and buoyant, but regularization removes such instability. If the buoyancy were to be realized, one would expect an entraining buoyant updraught to form with the possibility that entrainment on the radially-outward part of the (axisymmetric) cloud would be sufficient to reverse the low-level outflow associated with near-surface friction to produce inflow above the friction layer leading to vortex spin up. This would be the classical vortex spin up mechanism at work (see e.g., Smith and Montgomery 2023, Section 8.2).

As discussed in Montgomery and Smith (2022), regularization of the Eliassen equation so that it is globally elliptic has the consequence of preventing such inflow from occurring so that the vortex continues to spin down. Montgomery and Smith argued that vortex spin up in a hydrostatic model could be achieved only if deep convection were parameterized in a way that allows it to entrain air at larger radii above the boundary layer at a rate sufficient to produce inflow there. This argument is supported by the present findings using a balance model with explicit latent heat release.

4.3. Weaker initial vortices

We carried out two additional calculations with weaker initial vortices, one with $V_{max} = 20$ m s^{-1} and the other with $V_{max} = 10$ m s^{-1}. The configuration of these calculations was otherwise exactly the same, except that the time step for integration was extended to 5 minutes. The results are briefly as follows. Again, *both vortices decay* and the weaker the initial vortex, the longer is the time it takes for an elevated cloud to form, and the weaker is the overturning circulation at the time when cloud forms. Again, a shallow layer of fog forms in the inner core region before an elevated cloud forms. For the initial vortex with $V_{max} = 20$ m s^{-1}, an elevated cloud forms after about $3\frac{1}{2}$ hours and is confined below 3 km altitude until the calculation breaks down after about $9\frac{1}{2}$ hours. For the initial vortex with $V_{max} = 10$ m s^{-1}, a feeble elevated cloud forms after about $20\frac{1}{2}$ hours and never extends above 1.8 km altitude. In this case, the calculation does not break down during a 48 hour integration.

4.4. Solution breakdown

It is outside the scope of this study to explore the reasons for a complete breakdown of the solution for the evolving vortex at some time beyond that where regularization of the solution is required to advance the solution forwards. In fact, because the integrity of the solution in the region of regularization cannot be guaranteed, studies of the final breakdown would be of questionable value. Suffice it to say that the breakdown is different to that reported in Smith et al. (2018), where it appeared to be associated with a form of inertial instability that was not entirely suppressed by regularization. In that case, a negative radial gradient of absolute angular momentum remained in the prognostic equation for the tangential velocity. In the present case, the breakdown follows the development of convective instability, which *is* fully removed by regularization.

4.5. Summary of the main findings so far

The solutions presented herein highlight additional deficiencies of a strict balance model when extended to include explicit moist processes. Deficiencies of the dry model are discussed in Smith and Montgomery (2023), Section 8.4.5.

(1) The development of a strong vertical gradient of tangential wind near the surface on account of friction is accompanied by near-surface cooling, which leads to a shallow layer of fog. The cooling is an artefact of assuming thermal wind balance in the boundary layer. In turn, fog formation would serve to quickly suppress surface moisture fluxes from the ocean if these fluxes were included in the formulation. However, condensation in the foggy layer does not lead to convective instability.

(2) As soon as condensation occurs aloft, the coefficient multiplying the term $\partial^2\psi/\partial r^2$ in the moist Eliassen equation becomes negative and regularization is immediately required. This coefficient is proportional to the moist vertical stability of the elevated cloudy region, i.e., the cloud that forms is convectively unstable.

(3) The need to regularize the solution, to advance it beyond the stage at which convective instability occurs, removes such instability. Thus, regularization prevents the generation of local unbalanced buoyancy associated with convective instability, whereupon cloud formation in the moist model is passive and confined to shallow regions where the boundary layer forcing of ascent is strongest. There appears to be no way that deep clouds could form in the moist model unless, possibly, the atmosphere is nearly saturated through a deep layer initially. In a calculation starting from an initially saturated atmosphere, the solution suffers breakdown after the first time step. In that case, the moist Eliassen equation is globally hyperbolic at the initial time. It follows that *a moist balance model for tropical cyclone intensification intrinsically requires deep convection to be parameterized* to avoid the foregoing problem.

In retrospect, the second and third findings are essentially a rediscovery of the intrinsic moist convective instability of the tropical atmosphere (Bjerknes 1938, Lilly 1960), but in the context of an evolving vortex in the moist prognostic balance model.

The most important finding is that regularization of the moist Eliassen equation to make it globally elliptic, thereby allowing the solution to be advanced forwards in time, removes any convective instability. This removal has the unintentional effect of preventing the model clouds from generating inflow above the boundary layer. As a result, the vortex in the prognostic balance model with explicit latent heat release spins down.

Failure of the moist balance model to simulate an intensifying vortex might be interpreted as a negative result of our study, but it does provide an appropriate context for trying to reconcile the classical theories of tropical cyclone intensification and the WISHE-theories.

5. Implications for the WISHE theories

Like the prognostic balance model described in Section 2, the Emanuel (1995, 1997, 2012) models that are purported to underpin the WISHE intensification theory assume both hydrostatic balance and gradient wind balance of the tangential velocity, v. However, the WISHE-theories incorporate a different representation of moist processes and, importantly, they represent the surface moisture source explicitly.

5.1. Congruence assumption

Although there are differences in detail, all the WISHE-theories are based on the premise that, above the frictional boundary layer, there is congruence of the surfaces of absolute angular momentum, M, and those of saturation moist entropy, or equivalently the saturation equivalent potential temperature, θ_e^*, globally and at all times. Notably, the only prediction equation in these theories is for the moist entropy, or equivalently θ_e. If near-surface values of θ_e increase in the inner-core region on account of an increase in the surface enthalpy fluxes, then, the M-surfaces would be slaved to move inwards above and at the top of the boundary by the congruence assumption.

Significantly, the flow configuration of the WISHE-theories is almost identical to that in the moist balance formulation of Section 2, in which, without an explicit parameterization of deep convection, the vortex spins down on account of radial outflow induced by boundary layer friction. *What then enables the vortex to spin up in the WISHE-theories*? Clearly, the spin up of the tangential flow *above the boundary layer* can occur only by the vertical advection of M on account of the negative vertical gradient of M there. However, this argument does not explain physically how the maximum tangential wind, V_{max}, amplifies with time. Since the vertical gradient of M must be positive in the (balanced) frictional boundary (or zero if the boundary layer is assumed to be vertically well mixed at leading order), V_{max} must occur at the top of the boundary layer and the only way it can increase is if the M-surfaces move inwards at this level. Further, since M is assumed to be materially conserved at the top of the boundary layer as well as above it, there must be inflow at the top of the boundary layer to move M-surfaces inwards.

With the assumption of outflow just above the boundary layer, the inflow at the top of the boundary layer implies the existence of a sheet of azimuthal vorticity at this level. The question then is: what physical mechanism gives rise to the inflow at the top of the boundary layer in such a vortex sheet? It would seem that the inflow has to be a result of the assumed congruence between the M- and saturation moist entropy surfaces at the boundary layer top, but is this mechanism physically realistic? An analysis of azimuthally-averaged fields from a three-dimensional simulation of tropical cyclone intensification does not support the congruence assumption during much of the intensification stage. Only as the mature stage is reached (based on a levelling off of the maximum wind speed) is the assumption approximately valid and only then in the eyewall and outflow region (Smith and Montgomery 2023, Section 12.5). Indeed, we would argue that a more robust approach in any model for spin-up would be to determine the tangential velocity by solving the tangential momentum equation, or equivalently the prognostic equation for M, rather than using this equation to infer the *radial* motion in conjunction with the congruence assumption, as in the WISHE-theories (e.g., Peng et al. 2018 Eqs. (A13) and (A14))[§].

As shown in the Appendix 1, the assumed congruence between the M- and saturation moist entropy surfaces is equivalent to assuming that the moist saturated potential vorticity, P_m^*, defined as

$$P_m^* = \frac{(\boldsymbol{\omega} + \mathbf{f}) \cdot \nabla \theta_e^*}{\rho}, \tag{15}$$

is identically zero. It is shown in Appendix 2 that, unlike in the dry case, where the dry PV defined by

$$P = \frac{(\boldsymbol{\omega} + \mathbf{f}) \cdot \nabla \theta}{\rho} \tag{16}$$

is functionally proportional to the discriminant D given by Eq. (7), P_m^* is not functionally proportional to D_m given by Eq. (11). In other words, in the dry case, zero PV coincides with zero D, but in saturated air, zero P_m^* implies that D_m is negative, i.e., in saturated air, the moist Eliassen equation is *hyperbolic*[¶]. Thus, the assumed congruence in the moist problem implies that it cannot be interpreted in a similar balance framework as in the classical theories. In the latter theories, the Eliassen equation for the overturning circulation is elliptic.

Since the WISHE-theories make the same balance and congruence assumptions as above and since they have a similar flow configuration with outflow above the boundary layer, it would appear that these are irreconcilable with the classical theories also. A further reason for the incompatibility between the WISHE-theories and the classical theories is discussed in Subsection 5.3 below.

[§]In contrast to the deductions made above concerning the amplification of V_{max} at the top of the boundary layer, and the requirement of inflow in a sheet at this level, Peng et al. assume that the radial flow is zero there (see their Fig. 10b). If this were the case, there would be no mechanism to increase the radial pressure gradient at the boundary-layer top and therefore, on the basis of boundary layer dynamics, through the depth of boundary layer as well. Then, there would be no way to increase the boundary layer inflow and therefore, no way to amplify V_{max}!

[¶]It may be worth noting that this conclusion is different to that for moist Eady problem of baroclinic instability in a slab-symmetric, semi-geostrophic framework worked out by Emanuel et al. (1987). These authors derive a relationship between the diabatic heating rate and the dry and moist saturation potential vorticities, indicating that the slantwise, moist neutrally-stable state coincides *exactly* with the condition that the moist saturated potential vorticity is zero. While we have verified that such a condition is valid also for neutral slantwise stability of the moist Eliassen problem studied here, we note that Emanuel et al. make several approximations in their derivation: besides approximate cross-front geostrophic balance and hydrostatic balance, other assumptions include (i) the use of geostrophic (pseudo-) height, (ii) the approximation that the vertical velocity in pressure coordinates is proportional to the vertical velocity in the assumed height coordinate, (iii) the assumption that density is a constant, and (iv) that the "r" parameter is spatially and temporally constant. In contrast, besides the hydrostatic and gradient wind balance approximations, in the moist Eliassen model we make only the approximation that the local tendency of saturation mixing ratio is small compared with the advective tendencies when calculating the latent heat release. Moreover, it should be noted that the condition for slantwise neutral moist stability need not be identical to the discriminant condition for ellipticity in the moist balance model. The former is a condition for the stability of axisymmetric rings displaced from their equilibrium configuration. The latter is a condition for the Eliassen equation governing the secondary circulation of a slowly evolving vortex to remain elliptic. We know of no principal of physics that requires these conditions to be the same.

5.2. Ventilation issues

Insights from the moist balance formulation of Section 2 raise questions also about the configuration of the WISHE-theories, in which congruent M- and θ_e^*-surfaces emanate from the inner-core boundary layer and rise to the upper-troposphere at all stages of vortex evolution. In reality, the vertical extent of convection depends on a number of factors, in particular, the effective buoyancy in the convection (Smith and Montgomery 2022), but in the balance theories under discussion, there is no local unbalanced buoyancy by definition. With this perspective, it is unclear how the foregoing configuration could become established, starting from an initially weak vortex in an unsaturated atmosphere as in Section 2. Moreover, as demonstrated in Smith et al. (2021), it cannot be assumed *a priori* that all air exiting the boundary layer can be ventilated by buoyant deep convection. We note that this ventilation issue is not a feature of the classical theories (Smith and Wang 2018). We note also that the classical theories do predict inflow throughout the lower troposphere as is found in observations and in analyses of three-dimensional model simulations of intensifying tropical cyclones (Smith and Montgomery 2023, Chapters 1 and 11).

5.3. A fundamental question

The attempt to reconcile the WISHE-theories and the classical theories highlights an important question concerning the assumed flow configuration in the WISHE-theories. The implied diabatic heating rate in these theories associated with ascent along saturation moist adiabats has presumably a spatial distribution similar to that assumed in the classical theories with a maximum heating rate in the middle troposphere. In the classical theories, the spatial gradients of this heating rate distribution induce inflow below the heating rate maximum, which is well above the boundary layer. The question is, why does this heating distribution not induce a similar inflow in the WISHE-theories?

6. Conclusions

We have sought to reconcile the classical axisymmetric balance theories of tropical cyclone intensification by Shapiro and Willoughby and Schubert and Hack with the various WISHE-models of Emanuel. Since a scale analysis suggests that axisymmetric balance models provide a zero order foundation for understanding tropical cyclone behavior, it would seem important to know how these two theories relate and which, if either, of these theories is most useful for providing understanding? This endeavour necessitated an extension of the classical theories to account for explicit latent heat release in slantwise ascending air. The extension uncovered enroute a range of old modelling issues concerning the representation of deep convection in a balance framework and reaffirmed the need to parameterize buoyant deep convection in order to obtain a theory for intensifying storms.

The behaviour of the extended moist model with explicit latent heat release is illustrated by a particular calculation starting with an axisymmetric vortex in a conditionally-unstable atmosphere. In this calculation, the flow becomes convectively unstable as soon as condensation occurs aloft and the moist Eliassen equation for the balanced secondary circulation becomes hyperbolic in the convectively-unstable region. The solution can be extended beyond this time by regularizing the moist Eliassen equation to remove the hyperbolic region, but regularization removes any convective instability. Moreover, the regularized solution becomes noisy after some time and for strong initial vortices eventually breaks down. The suppression of convective instability removes any mechanism to produce inflow in the lower troposphere in the presence of the frictionally-induced outflow there. Such inflow would be required to draw absolute angular momentum surfaces inwards above the boundary layer to enable vortex spin up. As a result, the initial vortex progressively decays, even following the formation of elevated cloud with the accompanying latent heat release.

We showed that in the extended moist model, the development of a strong vertical gradient of tangential wind near the surface on account of friction is accompanied by strong near-surface cooling, which leads to a shallow layer of fog. The cooling is an artefact of assuming strict thermal wind balance in the boundary layer. The formation of fog would turn off surface moisture fluxes from the ocean had these fluxes been included in the formulation. We showed that, because of the strong cooling, the condensation in the foggy layer does not lead to convective instability.

Since the flow configuration of the extended prognostic model is similar to that in the WISHE-theories, the model and its solution behaviour provide a suitable framework in which to attempt a reconcilliation of the classical theories and the WISHE-theories. In particular, the comparison of the two theories poses a fundamental question: how does the maximum tangential wind, V_{max}, in the WISHE-theories amplify when the flow above the boundary layer is assumed to be everywhere outwards? We traced the reason for this amplification to a core assumption of the WISHE-theories that the surfaces of saturation moist entropy and absolute angular momentum are everywhere congruent above and at the top of the boundary layer, implying that the moist saturation potential vorticity is identically zero. With moist entropy as the prognostic variable in these theories, the absolute angular momentum surfaces are dragged inwards as a result of being slaved to the moist entropy surfaces by the congruence assumption.

A related question addressed is the location of V_{max}. We argued that V_{max} must occur at the top of the boundary layer, at which level there must be inflow, and that the spin up above the boundary layer top must occur through the vertical advection of absolute angular momentum as the radial flow there is outwards. As saturated air parcels ascend above the boundary layer in the WISHE-theories, while conserving their moist entropy, the accompanying diabatic heating rate must have a similar spatial distribution to that assumed in the classical theories. This fact leads to fundamental questions: why would this heating distribution not produce inflow above the boundary layer in the WISHE-theories as in the classical theories? And why is the diabatically-induced inflow restricted to a sheet of azimuthal vorticity at the boundary layer top? We noted that, in an azimuthal average of observations and three-dimensional models, there is inflow throughout much of the lower troposphere during the intensification phase. Such inflow is a feature also of the classical spin up theory.

While an intensification of the tangential velocity at the top of the boundary layer in the WISHE-models will lead

through elementary boundary layer dynamics to increased inflow in the boundary layer, we pointed out that there is no reason to suppose that all the inflowing air could be ventilated to the upper troposphere by the implied heating rate distribution. We noted that the classical intensification theories do not make the assumption that the flow rising out of the boundary layer is automatically ventilated to the upper troposphere.

At the core of the classical axisymmetric balance theories is a second-order partial differential equation for the streamfunction of the overturning circulation, the so-called Eliassen equation, which is elliptic provided that the product of the absolute vertical rotation rate and the dry potential vorticity is globally positive. An important new finding of our analysis is that, unlike in the dry problem, the discriminant of the corresponding moist Eliassen equation is not functionally proportional to the saturation potential vorticity. Moreover, we showed that if the surfaces of saturation moist entropy and absolute angular momentum are congruent, as in the WISHE-theories, the discriminant of the moist Eliassen equation is negative, in which case, the equation is hyperbolic. For this reason alone, *it was argued that it is not possible to reconcile the classical intensification theories and the WISHE-theories*. It was argued also that, *from a physical perspective, the spatial distribution of diabatic heating rate in the WISHE theories would be such as to induce inflow in the lower troposphere above the boundary layer in the classical theories instead of outflow there as postulated in the WISHE-theories, themselves*.

In summary, our attempt to carry out a reconciliation of the classical intensification theories and the WISHE-theories has uncovered a range of questions about the WISHE-theories, themselves, that we are unable to answer, but which call into question the integrity of these theories. In particular, we noted evidence showing that the global congruence assumption of the WISHE-theories is not a feature of azimuthally-averaged fields from three-dimensional tropical cyclone simulations, nor, to our knowledge, is it supported by observations.

Acknowledgements

We thank Kerry Emanuel for his perceptive comments on an earlier version of the manuscript.

References

Dunion, J. P., 2011: Rewriting the climatology of the tropical north atlantic and caribbean sea atmosphere. *J. Clim.*, **24**, 893–908.

Eliassen, A., 1951: Slow thermally or frictionally controlled meridional circulation in a circular vortex. *Astrophys. Norv.*, **5**, 19–60.

Eliassen, A., 1962: On the vertical circulations in frontal zones. *Geofys. Publ.*, **24**, 147–160.

Emanuel, K. A., 1995: The behavior of a simple hurricane model using a convective scheme based on subcloud-layer entropy equilibrium. *J. Atmos. Sci.*, **52**, 3960–3968.

Emanuel, K. A., 1997: Some aspects of hurricane inner-core dynamics and energetics. *J. Atmos. Sci.*, **54**, 1014–1026.

Emanuel, K. A., 2012: Self-stratification of tropical cyclone outflow. Part II: Implications for storm intensification. *J. Atmos. Sci.*, **69**, 988–996.

Emanuel, K. A., M. Fantini, and A. J. Thorpe, 1987: Baroclinic instability in an environment of small static stability to slantwise moist convection. Part I: Two-dimensional models. *J. Atmos. Sci.*, **44**, 1559–1573.

Möller, J. D., and L. J. Shapiro, 2002: Balanced contributions to the intensification of hurricane opal as diagnosed from a GFDL model forecast. *Mon. Wea. Rev.*, **130**, 1866–1881.

Montgomery, M. T., and J. Persing, 2020: Does balance dynamics well capture the secondary circulation and spinup of a simulated hurricane? *J. Atmos. Sci.*, **78**, 75–95.

Montgomery, M. T., and R. K. Smith, 2022: Minimal conceptual models for tropical cyclone intensification. *Tropical Cyclone Research and Review*, **11**, 61–75.

Peng, K., R. Rotunno, and G. H. Bryan, 2018: Evaluation of a time-dependent model for the intensification of tropical cyclones. *J. Atmos. Sci.*, **75**, 2125–2138.

Schubert, W. H., and B. T. Alworth, 1982: Evolution of potential vorticity in tropical cyclones. *Quart. Journ. Roy. Meteor. Soc.*, **39**, 1687–1697.

Schubert, W. H., and J. J. Hack, 1982: Inertial stability and tropical cyclone development. *J. Atmos. Sci.*, **39**, 1687–1697.

Schubert, W. H., and J. J. Hack, 1983: Transformed Eliassen balanced vortex model. *J. Atmos. Sci.*, **40**, 1571–1583.

Shapiro, L. J., and H. Willoughby, 1982: The response of balanced hurricanes to local sources of heat and momentum. *J. Atmos. Sci.*, **39**, 378–394.

Smith, R. K., 2006: Accurate determination of a balanced axisymmetric vortex. *Tellus A*, **58**, 98–103.

Smith, R. K., G. Kilroy, and M. T. Montgomery, 2021: Tropical cyclone life cycle in a three-dimensional numerical simulation. *Quart. Journ. Roy. Meteor. Soc.*, **147**, 3373–3393.

Smith, R. K., and M. T. Montgomery, 2022: Effective buoyancy and cape: some implications for tropical cyclones. *Quart. J. Roy. Meteor. Soc.*, **148**, 2118–2131.

Smith, R. K., and M. T. Montgomery, 2023: *Tropical cyclones: Observations and basic processes*. Elsevier, London, 411pp.

Smith, R. K., M. T. Montgomery, and H. Bui, 2018: Axisymmetric balance dynamics of tropical cyclone intensification and its breakdown revisited. *J. Atmos. Sci.*, **75**, 3169–3189.

Smith, R. K., and S. Wang, 2018: Axisymmetric balance dynamics of tropical cyclone intensification: Diabatic heating versus surface friction. *Quart. Journ. Roy. Meteor. Soc.*, **144**, 2350–2357.

Wang, S., and R. K. Smith, 2019: Consequences of regularizing the Sawyer-Eliassen equation in balance models for tropical cyclone behaviour. *Quart. Journ. Roy. Meteor. Soc.*, **145**, 3766–3779.

Wang, S., and R. K. Smith, 2021: Solutions of the eliassen balance equation for inertially and/or symmetrically stable and unstable vortices. *Quart. Journ. Roy. Meteor. Soc.*, **145**, 2760–2771.

Willoughby, H. E., 1979: Forced secondary circulations in hurricanes. *J. Geophys. Res.*, **84**, 3173–3183.

7. Appendix 1: Saturation moist PV

The saturation moist potential vorticity (moist PV) is defined by Eq. (15). For a symmetric vortex with tangential wind speed distribution $v(r,z)$,

$$\boldsymbol{\omega}+\mathbf{f}=-\frac{\partial v}{\partial z}\mathbf{i}+(\zeta+f)\mathbf{k}=-\frac{1}{r}\frac{\partial M}{\partial z}\mathbf{i}+\frac{1}{r}\frac{\partial M}{\partial r}\mathbf{k},$$

and

$$\nabla\theta_e^*=\frac{\partial\theta_e^*}{\partial r}\mathbf{i}+\frac{\partial\theta_e^*}{\partial z}\mathbf{k},$$

so that

$$P_m^*=\frac{1}{r\rho}\left(-\frac{\partial M}{\partial z}\frac{\partial\theta_e^*}{\partial r}+\frac{\partial M}{\partial r}\frac{\partial\theta_e^*}{\partial z}\right)=\frac{1}{r\rho}\mathbf{j}\cdot\nabla\theta_e^*\wedge\nabla M. \tag{17}$$

In the above formulae for $\boldsymbol{\omega}+\mathbf{f}$ and $\nabla\theta_e^*$, $\mathbf{i}$ and $\mathbf{k}$ denote unit vectors in the radial and vertical directions, respectively. It follows that zero moist PV is a situation that is equivalent to the congruence of the M-surfaces and θ_e^*-surfaces.

8. Appendix 2: Relation between P_m^* and D_m

Note that the formula for P_m^* (17) does not depend on any approximation for θ_e^*. Alternatively, we could write

$$P_m^* = \frac{\theta_e^*}{r\rho}\mathbf{j}\cdot\nabla\ln\theta_e^*\wedge\nabla M. \tag{18}$$

Since, typically, $\nabla\ln\theta_e^*$ is directed downwards and ∇M is directed outwards, P_m^* is mostly negative. Now

$$\ln\theta_e^* = \ln\theta + L_v r_v^*/(c_pT) = -\ln\chi + L_v r_v^*/(c_pT)$$

and, treating $L_v/(c_pT)$ as a constant to a first approximation, we can write

$$\frac{1}{\theta_e^*}\nabla\theta_e^* = -\frac{1}{\chi}\nabla\chi + \frac{L_v}{c_pT}\nabla r_v^*.$$

so that

$$P_m^* = \frac{\theta_e^*}{\rho}\left[-\frac{\partial v}{\partial z}\left(-\frac{1}{\chi}\frac{\partial\chi}{\partial r}+\frac{L_v}{c_pT}\frac{\partial r_v^*}{\partial r}\right)+(\zeta+f)\left(-\frac{1}{\chi}\frac{\partial\chi}{\partial z}+\frac{L_v}{c_pT}\frac{\partial r_v^*}{\partial z}\right)\right]. \tag{19}$$

Upon multiplying P_m^* by $g\rho\xi/\theta_e^*$ yields with a little algebra

$$\frac{g\rho\xi}{\theta_e^*}P_m^* = \left(I_g^2 - \frac{CL_v}{c_pT}\frac{\partial r_v^*}{\partial r}\right)\left(N^2+\frac{gL_v}{c_pT}\frac{\partial r_v^*}{\partial z}\right) - \left(B-\frac{CL_v}{c_pT}\frac{\partial r_v^*}{\partial z}\right)\left(B+\frac{gL_v}{c_pT}\frac{\partial r_v^*}{\partial r}\right), \tag{20}$$

where I_g^2, N^2, B^2 and γ are defined in Subsection 2.1. Subtracting the formula (20) from formula (11) divided by $4\gamma^2$ gives

$$\frac{D_m}{4\gamma^2} - \frac{g\rho\xi}{\theta_e^*}P_m^* = \left(B-\frac{CL_v}{c_pT}\frac{\partial r_v^*}{\partial z}\right)\left(B+\frac{gL_v}{c_pT}\frac{\partial r_v^*}{\partial r}\right) - \left\{B+\frac{L_v}{2c_pT}\left(g\frac{\partial r_v^*}{\partial r}-C\frac{\partial r_v^*}{\partial z}\right)\right\}^2, \tag{21}$$

which, after a little more algebra reduces to

$$\frac{D_m}{4\gamma^2} - \frac{g\rho\xi}{\theta_e^*}P_m^* = -\frac{1}{4}\left(\frac{L_v}{c_pT}\right)^2\left(g\frac{\partial r_v^*}{\partial r}+C\frac{\partial r_v^*}{\partial z}\right)^2. \tag{22}$$

Finally, using the fact that $r_v^* = r_v^*(p,T)$ and recalling that $g\partial p/\partial r + C\partial p/\partial z = 0$, in essence because the isobars are the characteristics of Eq. (3), it can be shown that

$$D_m = 4g\gamma^2\left[\frac{\rho\xi P_m^*}{\theta_e^*} - \underbrace{\frac{g}{4}\left(\frac{L_v}{c_pT}\right)^2\left(\frac{\partial r_v^*}{\partial T}\right)_p^2\left(\frac{\partial T}{\partial r}\right)_p^2}_{>0}\right]. \tag{23}$$

It follows from this expression that, if the M- and θ_e^*-surfaces are congruent, then $D_m < 0$, i.e., the moist Eliassen equation (10) is hyperbolic. Further details of the foregoing derivation may be obtained from https://www.meteo.physik.uni-muenchen.de/~roger/M42B_derivations.